

University of Massachusetts Boston

ScholarWorks at UMass Boston

Graduate Masters Theses

Doctoral Dissertations and Masters Theses

8-31-2017

Plasmonic Enhancement of Organic Light Emitting Diodes (OLEDs) with Periodic and Random Nanostructures

Pavel Markeev

University of Massachusetts Boston

Follow this and additional works at: https://scholarworks.umb.edu/masters_theses



Part of the [Physics Commons](#)

Recommended Citation

Markeev, Pavel, "Plasmonic Enhancement of Organic Light Emitting Diodes (OLEDs) with Periodic and Random Nanostructures" (2017). *Graduate Masters Theses*. 454.

https://scholarworks.umb.edu/masters_theses/454

This Open Access Thesis is brought to you for free and open access by the Doctoral Dissertations and Masters Theses at ScholarWorks at UMass Boston. It has been accepted for inclusion in Graduate Masters Theses by an authorized administrator of ScholarWorks at UMass Boston. For more information, please contact scholarworks@umb.edu.

PLASMONIC ENHANCEMENT OF ORGANIC LIGHT EMITTING DIODES
(OLEDs) WITH PERIODIC AND RANDOM NANOSTRUCTURES

A Thesis Presented

by

PAVEL MARKEEV

Submitted to the Office of Graduate Studies,
University of Massachusetts Boston,
in partial fulfillment of the requirements for the degree of

MASTER OF SCIENCE

August 2017

Revised 2021

Applied Physics Program

© 2017 by Pavel Markeev
© 2021 revised by Pavel Markeev
All rights reserved

PLASMONIC ENHANCEMENT OF ORGANIC LIGHT EMITTING DIODES (OLEDs)
WITH PERIODIC AND RANDOM NANOSTRUCTURES

A Thesis Presented

by

PAVEL MARKEEV

Approved as to style and content by:

Maxim Olchanyi, Professor
Chairperson of Committee

Stephen Arnason, Associate Professor
Member

Chandra Yelleswarapu, Associate Professor
Member

Stephen Arnason, Program Director
Applied Physics Program

Bala Sundaram, Chairperson
Physics Department

ABSTRACT

PLASMONIC ENHANCEMENT OF ORGANIC LIGHT EMITTING DIODES (OLEDs) WITH PERIODIC AND RANDOM NANOSTRUCTURES

August 2017

Pavel Markeev, B.S., Ural Federal University, Yekaterinburg, Russia

M.S., University of Massachusetts Boston

Directed by Professor Maxim Olshanyi

This revised thesis has been submitted in 2021 due to findings of academic misconduct in the original thesis. The misconduct included improper citation and plagiarism of Dr. Khadir's PhD thesis [1], particularly in the introduction, the state of the art and images 1.1-1.6, 2.4, 3.2, 3.4.

The localized surface plasmon resonance (LSPR) is known as a phenomenon that allow to enhance the efficiency of Organic Light Emitting Diodes (OLED). This work researches the dependence of OLED performance with and without metallic nanoparticle incorporated in the organic layers. Diodes with periodic (PMN) and random (RMN) metallic nanoparticles along with both types of nanoparticles were compared to the reference OLED. Thermal evaporation technique was used to form organic layer under high vacuum and e-beam lithography to compose periodic metallic structures on nano scale. Reporting that periodic structure increases the luminescence and electrical properties of the device for approximately 20% but devices with both types of nanostructures demonstrated 50% decrease of efficiency.

ACKNOWLEDGMENTS

I am indebted to Professors Maxim Olshanii, Chandra Yelleswarapu and Azzedine Boudrioua for their support over my lengthy stay in the master's program. Maxim suggested me to participate at an internship in University Paris 13 and helped a lot to with all preparational work. Chandra has been advising me how to get admission to the university and during the first year of my master program. Azzedine is the leader of physics laboratory at Paris 13 who was mentoring my entire work there and giving advices for getting better results out of my internship. Unfortunately, I was not being able to obtain new results out of my experiment that would be worth to be presented to the scientific society. I want to express my gratitude to Dr. Amadou Diallo and Dr. Samira Khadir for all the support they provided me during the internship. This feeble acknowledgment can scarcely express my gratitude. Thank you!

TABLE OF CONTENTS

ACKNOWLEDGMENTS	v
LIST OF FIGURES	vii
CHAPTER	Page
INTRODUCTION	1
1. PRINCIPLES OF OLED AND PLASMONICS	3
1.1 History of OLEDs and Organic Semiconductors	3
1.2 OLED structure and operation principle	5
1.3 Energy transfer in OS	9
1.4 OLED degradation	9
1.5 Localized Surface Plasmon Resonance	10
1.6 Effect of MN parameters on the LSPR	12
2. SIMULATIONS OF THE LSPR	16
2.1 Theory of FDTD	16
2.2 FDTD simulations	17
3. METHODOLOGY AND RESULTS	20
3.1 OLED production and measurement	20
3.2 Fabrication of periodic nanostructures	23
3.3 Results and discussion	25
CONCLUSION	27
REFERENCE LIST	28

LIST OF FIGURES

Figure	Page
1.1. Efficiency development of white OLEDs (WOLED) over the period from 1995 to 2010	3
1.2. a) An example of interchange of single and double bonds in organic material	5
1.3. Schematic cartoon of OLED operation under positive bias: 1) Charge injection and 2) transport; 3) charge recombination; 4) exciton decay and photon emission	6
1.4. Schematic energy transfer by a) Förster and b) Dexter	9
1.5. Lifetime drop for devices with different initial luminance.....	10
1.6. Charge agglomeration along surface plasmon expansion.....	11
1.7. Localized plasmon surface resonance, left at the initial time, right at the time of half period.....	12
1.8. a) Extinction spectra of silver cylindrical nanoparticles with constant height of 2 nm and diameter of 2 nm (squares), 3 nm (circles), 4 nm (triangles), 6 nm (rhombus), 8nm (hexagons) and 10 nm (left-handed triangles)	13
1.9. Position of the main plasmon peak according to the size and shape	14
1.10. Dependence of extinction spectra on a) the material of MN [34] and b) the surrounding media refractive index.....	15
2.1. Electric and magnetic fields in the elementary cell of Yee model	16
2.2. The leapfrog method: time method of the Yee scheme	17
2.3. Periodic metallic particles covered by organic material	18
2.4 Simulation of LSPR for different size of silver NP	18
2.5. Simulation of LSPR for different periods of silver NP structures	19
3.1. Evaporation chamber	21
3.2. Scheme of 4 OLED devices on a single glass substrate	22
3.3. Structure of organic layers of the OLED	22
3.4. Design of the characterization setup for μ -OLEDs.....	23
3.5. (a) Summary diagram of e-beam lithography	24
3.6. (a) Extinction cross-section of silver nanoparticles with different periods.....	25

Figure	Page
3.7 (a) Current density and (b) luminance as a function of the voltage for the μ -OLEDs with and without Ag NPs	26
3.8. Luminous efficiency as a function of current density (left), image of the reference red OLED (right).....	26

INTRODUCTION

Plasmonic effects is a rapidly expanding field of research and development in recent years. Such effects could be found at the crossroads of physics, chemistry and biology. These processes can be only studied with a deep understanding of the nano-world from different perspectives. From the physics point of view it is important to know and understand fields like optical and electronic lithography and nano-printing to produce devices with plasmonic effects. On the other hand, the research is not possible without the opportunity to synthesize nano-objects by reduction of metallic compounds and organometallic precursors. Lastly, the findings can be then applied in numerous spheres in biology, health, energy and sustainability. Plasmonics quickly evolve towards increase of functionality and ways of application by usage of the concept of localized surface plasmon (LSP) which appears at nano sized metal nanoparticles.

This work is focused on enhancing the efficiency of organic light emitting diodes (OLED) using structures of metallic nanoparticles (MN). The MN structure allows the localized plasmon to enter the resonance state by coupling with the emitted light from OLED. This resonance state called localized surface plasmon resonance(LSPR). The LSPR is an area of plasmonics that has been studied for several decades. Surface plasmon is a oscillation of free electron cloud on the interface of metal and dielectric or semiconductor [2]. When the metal is presented by a thin film or a small enough particle then the electromagnetic field can penetrate the metal and the created plasmon would be localized. The size of the metallic nanoparticle needs to be so the field can fully penetrate it. The localized plasmon fluctuations can be described as a harmonic oscillator, which also can enter the resonance state. Hence the LSPR can enhance the emitted light from OLED [1].

OLED devices in analogy to inorganic light emitting devices operate on the principle of electroluminescence [3]. The internal efficiency of the OLEDs luminescence is limited by quantum laws up to 25%. The 25% are the excitons created in singlet state, the rest of excitons are in the triplet state. Only singlet state exciton can radiatively deexcite and emit a photon, radiative deexcitation for the triplet state is spin-forbidden. There were created new ideas to enhance the performance of OLED, by means of for examples LSPR. If the distance between the emitting layer in the OLED and MN is small enough, then the light emission will be increased due to LSP resonance [4].

In this work we produced and studied OLEDs with two different metallic nanostructures and compared them to the reference OLED. The first type is a device with periodic nanoparticles on the side of anode relatively to the emitting layer, the second type has periodic particles on the same side and random metallic particles on the other side from the emitting layer. Before the device production additional computer simulations have been carried out to better understand the LSPR. Even though the results of simulations are slightly different from the obtained experimental results, they provided interesting and important insights before device preparation. It was decided to use 100 nm silver cylindrical nanoparticles in the nanostructures.

This thesis is divided into 3 chapters. The first chapter provides the literature review of theory behind OLEDs and the LSPR. The operating principle, structure and manufacturing process of OLEDs are presented. The theory of LSPR with detailed literature review of factors that affect the LSPR are introduced in the same chapter. Second chapter is dedicated to the simulation data. There is a short overview of the calculational method and results of the simulations. The last chapter focuses on the experimental part of this work: methodology, challenges and results.

CHAPTER 1

PRINCIPLES OF OLED AND PLASMONICS

1.1 History of OLEDs and Organic Semiconductors

First work on organic semiconductors (OS) electrical and optical properties started back in the 50s of the previous century [5]. One of the first works that showed electroluminescence in such materials was Pope et al [6]. Their work was focused on anthracene single crystal, electroluminescence was observed for 10 to 20 μm thick crystal after applying 400 V potential difference to relatively small circular electrodes of 1 mm diameter, which represented current density around $100 \mu\text{A}/\text{cm}^2$. Such high voltage and low electroluminescence was far from real world application for the studied devices. The first publication of modern-like devices with promising properties can be credited to Tang and van Slyke at Kodak research laboratory [3]. They presented a diode with 75 nm aromatic diamine and 60 nm 8-hydroxyquinoline aluminum (Alq_3) as an emission layer, Indium Tin oxide (ITO) as an electrode on one side to release the light which is one of common transparent conducting oxides (TCO). The device demonstrated performance of 1.5 lm/W power efficiency operating under 10 V. Figure 1.1 compiles publication development results of white OLED performance over the period from 1994 to 2010 [4]. The improvement in OLED effectiveness is permanently growing over studied years and continues to grow to this date.

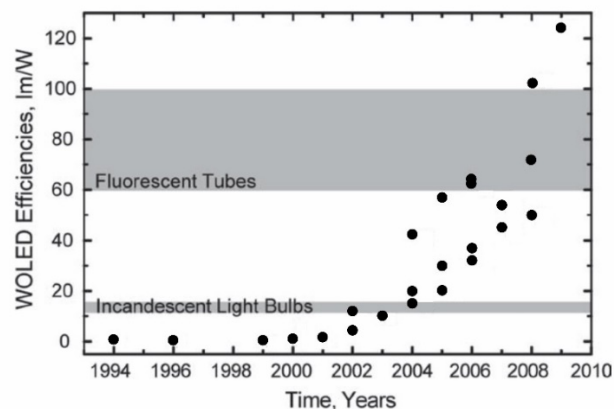


Fig. 1.1. Efficiency development of white OLEDs (WOLED) over the period from 1995 to 2010. Information for each data point, how it was measured and computed can be found in ref. [4]. Reproduced from ref. [4].

Organic semiconductors are materials that consist mostly of carbon, hydrogen and oxygen. There are two main features of OS which make them preferable instead of using

inorganic semiconductors in certain real world applications [1]. First, it is important to note that the melting point of a large number of organic materials used in OLED production is relatively low, below 350°C [7], [8]. This makes OS more accessible for production in lab conditions and allow to use the method of high-vacuum thermal evaporation for pure process and precise growth control. Second, OS are not oriented in the form of crystal lattice as most of inorganic semiconductors. After the evaporation OS are present in the form of an amorphous film, it makes them much more “soft” and elastic. Thanks to these properties, they can be used in flexible electronics and displays. Production of such devices is more suitable to study the plasmonic effect, the subject of this work.

There are 3 main categories of OS which can be utilized for OLED production: small molecules, polymers and dendrimers. In this work we use small molecules, because they provide more precise control over growth and allow the incorporation of metallic nanoparticles (NP) in the structure during one evaporation cycle. Small molecules mostly consist of a number of benzol rings and core metal atoms, such as Al in Alq₃ which is used as an emission layer in this work. OLEDs manufactured with polymer molecules are known as polymer light emitting diodes (PLED). Polymers cannot be evaporated in the same manner as small molecules and are commonly deposited by the spin-coating method [9]. It allows the production of larger areas covered by organic materials, but the thickness cannot be controlled as good as in thermally evaporated layers of small organic molecules. The last type of OS is receiving additional attention in recent years, dendrimers are highly oriented molecules consisting of core atoms in the symmetric center and polymeric branches [10]. The performance of the device can be precisely tuned by selecting the composition of dendrimers [11].

The semiconducting properties of OS arise from the chemical bonds of such materials. OS mostly include single and double bonds between carbon atoms. Interchange of these bonds provide semiconducting properties to the organics. An example of such interchange could be a chain of C atoms bound to each other or aromatic rings (Fig. 1.2). A bond between two carbon atoms can remain in two distinguished energy states: a highest occupied molecular orbital (HOMO) as a π bond and a lowest unoccupied molecular orbital (LUMO) as an anti-bonding π^* orbital [1]. In terms of solid physics and inorganic semiconductors the analogy of HOMO energy level would be the valence band where charge carriers are holes and LUMO would be the conduction band where charge carriers are represented by electrons.

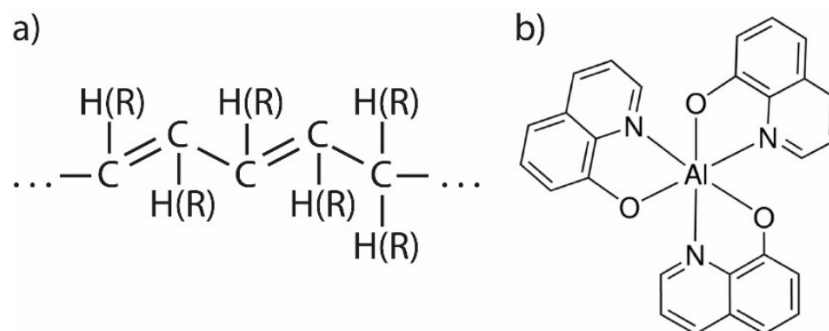


Fig. 1.2. a) An example of interchange of single and double bonds in organic material. (R) stands for a radical group. Reproduced from [1] b) Alq_3 as an example of such interchange within aromatic rings [3].

1.2 OLED structure and operation principle

In principle, as it was mentioned above, the first OLED devices consisted of only a single layer of organic material which served as an emission layer. Modern standards of OLED production include up to 7 thin layers stacked on top of each other. Each of these layers serves a designated function to improve the efficiency of the device [12]. The names of the layers are mostly self-explanatory. The charge injection to the stack of organic layers is done by means of two electrodes: Indium Tin Oxide (ITO) as an anode and an aluminum cathode. There are two layers to improve the charge injection from both “sides”: hole injection layer (HIL) and electron injection layer (EIL). The main reason for additional supporting layers around the emission layer (EL) is to provide an equal number of injected charges to the EL where the recombination and light emission occurs. For this task two more layers are utilized: hole transport layer (HTL) and electron transport layer (ETL). The last layer to discuss is hole blocking layer (HBL) which serves to decrease the waste of energy by stopping the holes that have not recombined in the EL [13]. HBL is located in between EL and ETL. This division is not obligatory to follow and some layers can be omitted. Omitting the layers may affect the performance, but the device will be fully operational.

Figure 1.3 assists to explain the process from charge injection to photon emission. The process is divided into 4 main steps. The charges, electrons and holes, are injected from corresponding electrodes. Anode is injecting holes and cathode – electrons. The crucial point about charge injection is to bring the work function of electrodes as close as possible to the HOMO and LUMO energy levels of the OS. Unfortunately, it is not possible, because the WF of metal cannot perfectly align with HOMO and LUMO, that is why additional injection layers (HIL and EIL) can be used. The following step after charge carriers were injected is to transport

them to the emission layer. The mobility attributes of electrons and holes do not match and it is important to adopt proper materials to achieve desired transport properties in HTL and ETL [13]. The injection and transport layers cooperate to provide needed amounts of holes and electrons in the emission layer. In the EL at step 3 an electron and a hole create a bonded pair – an exciton. The exciton then decays in a radiative manner and emits a photon. The emission happens only if the exciton is in the singlet form, which will be discussed later. The wavelength of the emitted photon is based on the properties of the material used in EL. This work uses doped ALQ₃ to produce red light OLED.

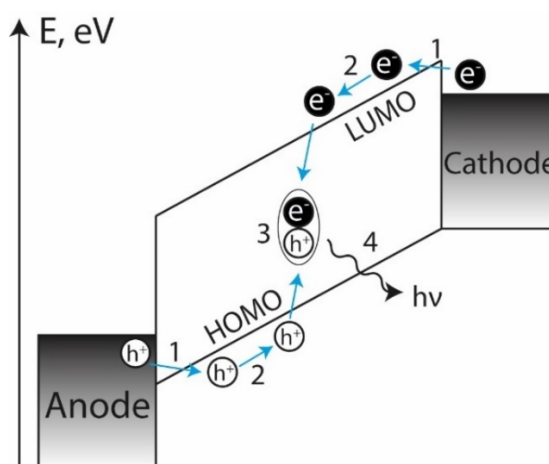


Fig. 1.3. Schematic cartoon of OLED operation under positive bias: 1) Charge injection and 2) transport; 3) charge recombination; 4) exciton decay and photon emission. Reproduced from [1].

Injection layers

As it was mentioned before, the injection layer serves for better charge carrier insertion to the OS from metal electrodes. This layer could be omitted if the WF of cathode would perfectly match HOMO level and WF of anode would match LUMO level of transport layers of the device. Unfortunately, this is not possible. The work function of ITO is reported between 4.4 to 4.7 eV [14], when HOMO level of ALQ₃ is at 5.5 eV [15]. The work function of other TCO lays in the same range, but ITO is one of the most commercially available and used materials for transparent electrodes. As HIL could be used different types of OS: 4'-tris{N,(3-methylphenyl)-N-phenylamino}-triphenylamine (m-MTDATA); 4,4',4'-tris{N,-(2-naphthyl)-N-phenylamino}-triphenylamine (2T-NATA); copper phthalocyanine (CuPc); and oxotitanium phthalocyanine (TiOPc). These 4 materials have been studied by Chen and Wang

[15] and m-MTDATA shows the most interesting results. In this work we use m-MTDATA as a HIL.

Common anodes that are used in OLEDs are made of aluminum, which has a WF around 4 eV, when LUMO level of Alq_3 is -2.4 eV [15]. It is not possible to use metals with such low WF as an electrode because of their high chemical activity. Several studies showed that a thin layer of lithium fluoride (LiF) improves electron insertion from Al anode [16], [17]. In this work Al anode with a thin layer of LiF is used for electron injection.

Transport Layers

The difference of electron and hole mobility in OS is certainly noticeable. Mobility of holes is at $10^{-4} \text{ cm}^2/(\text{V}\cdot\text{s})$ order of magnitude, when electron mobility is around $10^{-8} \text{ cm}^2/(\text{V}\cdot\text{s})$ [18]. Trapping process of electrons in organic molecules is much more probable to occur in comparison to holes to be trapped. It is important to use proper OS for electron transfer along with material for hole transfer to provide a balance of charge carriers in the EL. Using wrong materials or wrong thickness of transport layers can lead to overpopulation of the emission layer by one type of the carriers which will decrease the performance of the device. Another purpose of the transport layers is to bring the energy of the charge carriers as close as possible to HOMO and LUMO of the emission layer.

A lot of different organic materials have been studied for ETL, for example: poly(ethylene oxide) (*PEO*) [19], Alq_3 [20]. Alq_3 was used as ETL in this work. The materials, which could be used for HTL: Poly(N-vinylcarbazole) (*PVK*), poly(styrenesulfonate) (*PEDOT:PSS*), poly(3,4-ethylenedioxythiophene) [19], (N, N-diphenyl-N, N-bis (3-methylphenyl) - 1,1biphenyl-4,4-diamine) (*TPD*) and (N, N' -di (1-naphthyl)-N, N'-diphenyl- (1,1' biphenyl)-4,4'diamine) (*NPB*) [21], hydrazone [22]. *NPB* was chosen to be used as a HTL in this work.

Charge Blocking Layers

To avoid waste of energy and to keep the carriers within the emission layer, blocking layers for electrons and holes can be added. Electron blocking layer (EBL) could be added between EL and HTL, when HBL could be added in between EL and ETL. Along with the ability of stopping an opposite charge carriers, the blocking layers should perform high transport performance for the carriers depending on their position [13]. HBL must be able to stop holes, but also to pass electrons through itself on a high pace. Opposite can be applicable to the EBL. In the case of this work, the EBL was omitted because *NPB* serves not only as a

good transport layer for holes, but also sufficiently stops electrons [21]. BCP was chosen to use as a HBL in this work.

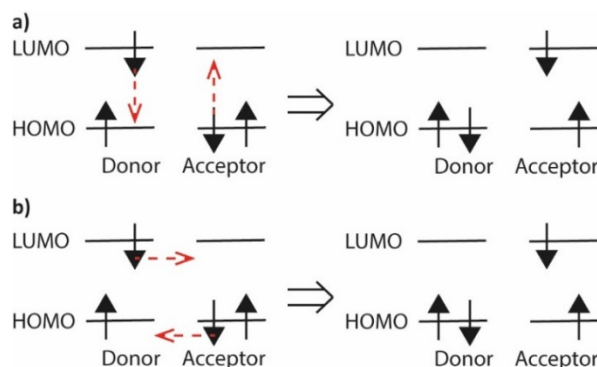
Emission layer

The number of materials that can be used as an emission layer is tremendous and the study and review of each of them could be a work for another master thesis. Here we provide a short overview of the materials for the EL. The most common way to divide and discuss the OS for EL is by the color of the light they emit. Producing white light in the OLED device is achievable by stacking 3 of different semiconductors, which will create the emission spectrum over the whole visible range. On the other hand, tuning each color and improving the performance of the certain light range is an advantage of OLEDs in comparison to the inorganic semiconductors [18]. Were developed different, precisely tuned OS for certain wavelength emission: as one example of green OLED emitting layer could be used 8 wt % Ir(ppy)₃ [fac-tris(2-phenylpyridine) iridium] doped with CBP [4,4'-N,N'-dicarbazole-biphenyl] [22]. To avoid enumeration of long names of organic materials, we would like to mention that the emission color of the OLED could be altered in a wider sense. Following the design of Tang [3] using Alq₃ with proper dopants can provide all colors from red to blue. Materials such as quinacridone, 9,10-diphenylanthracene, perylene and decacyclene can be used as dopants in Alq₃ to provide distinct colors and improve the lifetime of the device [22]. In this work Alq₃ doped with 4-(dicyanomethylene)-2-methyl-6-(p-dimethylaminostyryl)- 4H-pyran (DCM) was used to create a red OLED.

Emission layer is a location where recombination of charges happens. When electron and hole come to each other at a certain distance, for example, when they are located on the neighboring molecules, the exciton can be formed. Exciton is a bonded electron-hole pair, which is a quantum particle. In other sense, an exciton can be treated as an excited organic molecule, where this pair resides. Depending on the spin of the electron and the hole, a certain state of the exciton will be created. In one quarter of the time the singlet state will be formed. Other 75% will form a triplet state. Only singlet state can radiate a photon during deexcitation, radiation for a triplet excited state is spin forbidden [13]. This means that the theoretical limit of the efficiency for OLED devices is 25%. In reality such efficiency of electroluminescence is also hard to achieve due to other material problems in the device. There are works to improve OLEDs by overtaking this 25% efficiency limit by converting the triplet states into emitting singlets states [23].

1.3 Energy transfer in OS

It is important to understand how the energy is transferred in organic materials, because the mechanism is significantly different from energy transfer in inorganic semiconducting materials. The transfer of charge carriers could happen not only from a molecule to a molecule, but also from one to another part of a large organic molecule. But in a more general sense, one considers charge transfer from a molecule to a molecule. There are 2 main energy transfer methods in OS: Förster and Dexter, by the name of the scientists who suggested the theories [1]. Förster, also known as fluorescent resonant energy transfer (FRET) is a transfer of energy between 2 sites without direct transfer of electron (hole). The energy from the excited donor is transferred without radiation to the acceptor at a distance under 10 nm [24]. Dexter process is the process of direct transfer of the charge carrier from donor to the acceptor [25]. Hence, the distance of Dexter transfer is much smaller than Förster. The distance, at which the process can occur and the transfer rate can be calculated by the formulas presented in the following references [24], [25]. When donor and acceptor reach appropriate distance, the transfer process follows either the Förster or Dexter scenario. In the first the donor molecule deexcites to ground state and released energy which excites an electron in the acceptor molecule (Fig. 1.4a). In Fig. 1.4b the Dexter process is presented: the excited electron from the donor is transferred into the acceptor excited state, while the ground states also exchange electrons.



1.4. Schematic energy transfer by a) Förster and b) Dexter. Reproduced from [25].

1.4 OLED degradation

Despite all advantages of the OLED devices one of the main flaws is degradation of organic semiconductors. The performance of the devices could drop over long operation time or exposure to ambient conditions. The degradation from external factors, such as exposure to oxygen and water was thoroughly studied. The report in [26] shows that the lifetime of the device decreased more than 2 times when it was exposed to O₂. The exposure to water vapor is

1000 times more destructive in comparison to oxygen, where water destroys the electrode-OS connection [27]. Not only external factors, but OS do degrade from intrinsic changes over time as well. One of examples is drop of lifetime for devices with higher initial luminescence parameters (Fig. 1.5), another example – is the dependence of lifetime on the vacuum quality during the OLED production [28]. The increased injection barrier was studied in [29], due to lowering the quality of interfaces between different materials. It leads to an increasing number of trapping states, lower charge carriers mobility and device higher operational voltage. There are many other events that could happen in studied devices, depending on the type of organic molecules (small or polymers), fabrication method or chemical stability of the layers [22]. Figure 1.5 represent the lifetime drop for the devices with higher initial luminance.

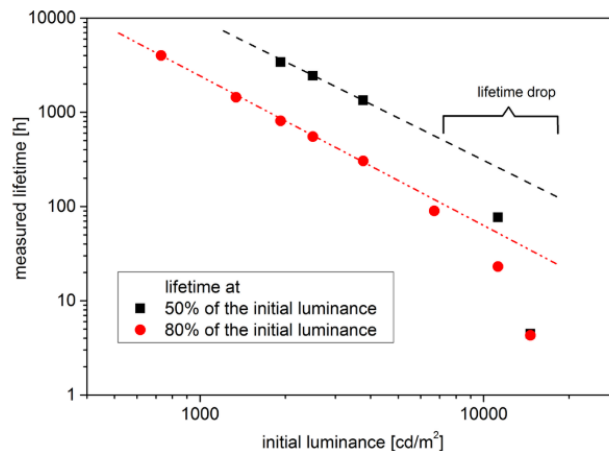


Fig. 1.5. Lifetime drop for devices with different initial luminance. The lifetime of the devices with higher initial luminance cannot be extrapolated as for devices with lower initial luminance [28].

1.5 Localized Surface Plasmon Resonance

In this work we study the performance of OLEDs by adding metallic nanoparticles (MN) into the device layers. The electroluminescence efficiency could be increased by achieving surface plasmon resonance within those particles. Surface plasmon (SP) is a fluctuation of electrons on the interface of conductor and insulator (or semiconductor) that function as a quasiparticle (Fig. 1.6) [2]. In simple words, surface plasmon is the consequence of the interaction between light and metal surface.

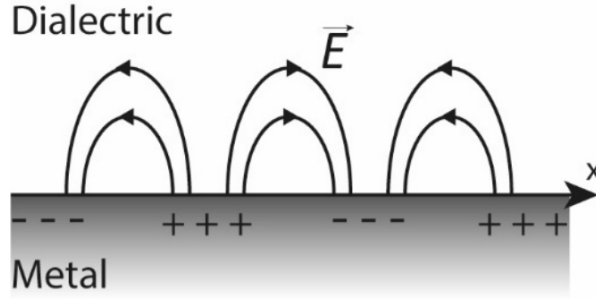


Fig. 1.6. Charge agglomeration along surface plasmon expansion. Reproduced from [2].

From the definition, one can conclude that such interaction is dependent on free electrons present in the metal, those electrons that can oscillate under the influence of the electromagnetic field. The interaction between the metal interface and the field can be described with Maxwell's equations. Solving the equations with proper boundaries allows one to find a wave-vector k_{sp} of the plasmon [2].

$$k_{sp} = k_0 \sqrt{\frac{\epsilon_d \epsilon_m}{\epsilon_d + \epsilon_m}} \quad (1.1)$$

The free space wave-vector is k_0 which is equal to ω/c . ϵ_d and ϵ_m are dielectric constants of the dielectric and the metal, respectively. The plasmon that travels along a metal dielectric interface is also sometimes called a delocalized plasmon. In normal situations without additional conditions, the coupling between light and SP is not possible, due to the wavenumber of photons being smaller than the wavenumber of SP [1]. If the metal is presented by a small particle (submicron size), the plasmon becomes localized and obtains some additional properties.

This phenomenon of electrons fluctuations inside small metallic particles is called localized surface plasmon LSP (Fig. 1.7). The electrons are shifted in the opposite direction from the incident electric field. The LSP is localized and does not propagate, which means it does not have a wavevector that follows the coupling and resonance between light and electron gas oscillations is achievable [1]. Simply illuminating MN will start the process and when the frequency of the light reaches the intrinsic frequency of the MN the system will enter the resonance: localized surface plasmon resonance (LSPR). The LSPR can assist to enhance the light emission from an OLED device.

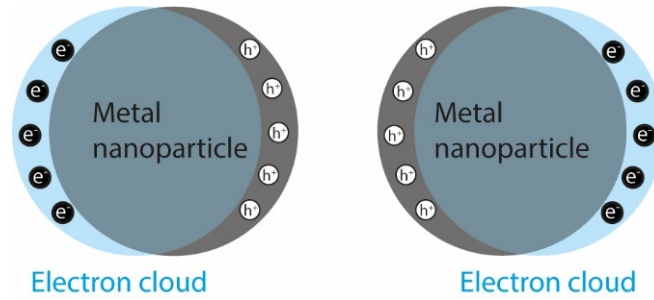


Fig. 1.7. Localized plasmon surface resonance, left at the initial time, right at the time of half period. Reproduced from [1].

The behavior of electron gas can be described as a classical problem of a harmonic oscillator. As any harmonic oscillator, this system can enter the resonance state, where the fluctuation amplitude of the electron cloud will exceed the incident electromagnetic field by a few times [30]. This demonstrates how such resonance in MN can enhance the light emission of the OLED. There are different methods, including the computational methods, to study the LSPR. Numerous publications discuss the effect of size, shape, used material and dielectric surroundings around the MN on the LSPR. First, the size will be discussed, because it is the easiest part of the experiment to alter, when the MN are produced by electron beam lithography, as in this work.

1.6 Effect of MN parameters on the LSPR

The size of the MN is one of the crucial aspects in tuning the LSPR for needed performance. To validate if the LSPR is tuned correctly, usually absorption or extinction is measured depending on the wavelength of the incident light. Amendola *et al.* [31] studied different aspects of metallic NP and their effect on the LSPR. One of the aspects is the size and ratio of cylindrically shaped silver particles. The extinction peak is increasing and shifts to the red spectra with increasing the diameter of the MN (Fig.1.8a). The diameter is starting from 2 nm for black curve with squares and reaches 10 nm in pink left handed triangles. The conditions surrounding the particle are kept the same with refractive index $n=1.43$. Most surprisingly, the paper claims that keeping the same ratio of the cylindrical particles, the LSP does not change and maintain constant (Fig. 1.8b). The LSPR is the same for particles of 2 nm diameter and 2 nm height as for 3 nm diameter and 3 nm height, *etc.* These results were obtained by the Mie model calculational method [32].

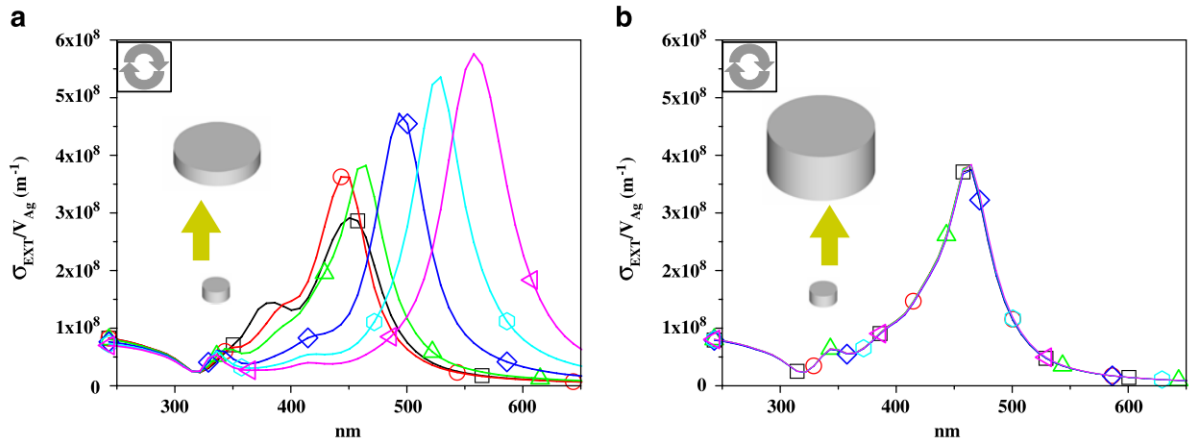


Fig. 1.8. a) Extinction spectra of silver cylindric nanoparticles with constant height of 2 nm and diameter of 2 nm (squares), 3 nm (circles), 4 nm (triangles), 6 nm (rhombus), 8 nm (hexagons) and 10 nm (left-handed triangles). b) Extinction spectra of silver cylindric nanoparticles with constant height diameter ratio of 2 nm diameter and 2 nm height (squares), 3 nm height and diameter (circles), 4 nm (triangles), 6 nm (rhombus), 8 nm (hexagons) and 10 nm (left-handed triangles). The surrounding media has $n=1.43$ [31].

Shape is the next crucial criterion of the MN to achieve desirable LSPR. The shape's effects were thoroughly studied by Mock *et al.* in silver particles [33]. The findings are summed up in the figure 1.9. The image provides the information about the center of the main peak of plasmon resonance according to the shape and size of the nanoparticle. The data points on the graph are grouped by the shape and within each group the peak experiences a red shift with enlargement of the particles. Spherical particles provide the LSPR peak from 400 to 500 nm, ranging according to the size: smaller particles (<50 nm) have a peak under 450 nm and larger ones (80 nm) – at almost 500 nm. Pentagon shaped MN peaks can be found in the range of 500 to 570 nm. The size cannot be well extrapolated for pentagons, most of the particles of size 80-100 nm exhibit peak at 520 nm. The higher end of spectra is occupied by triangular shaped MN. The particles of 50-70 nm represent 550 nm plasmon peak, when the peak of triangular particles larger than 80 nm can be found around 650 nm. As one can see, the shape and size play a crucial role in the development of the LSPR.

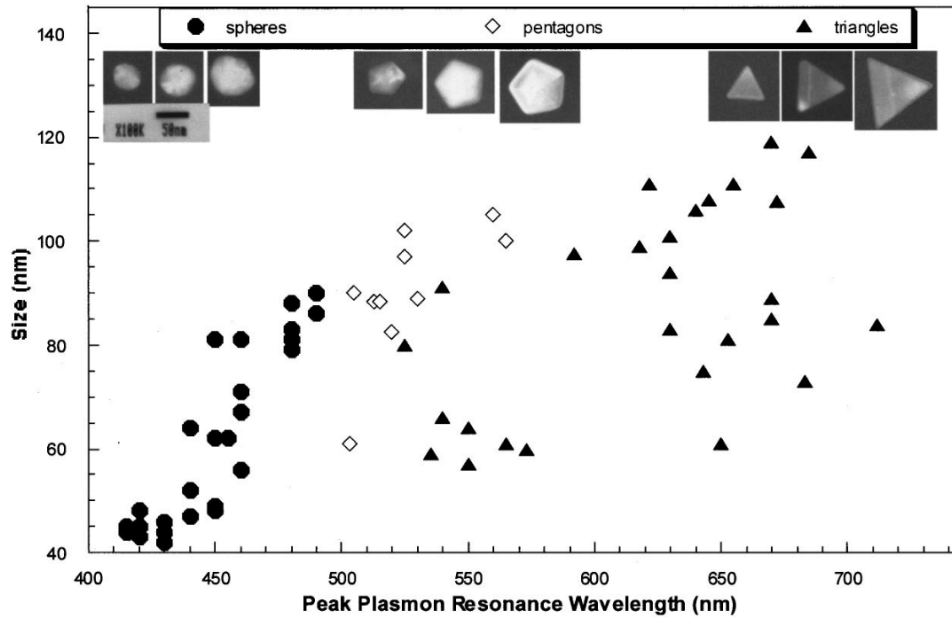


Fig. 1.9. Position of the main plasmon peak according to the size and shape. Circle – spherical shape MN, rhombus – pentagon shape, triangle – triangular shape [33].

Last two influential parameters on the LSPR peak position are the material from which the MN are made and the surrounding media, which in case of OLED is organic materials. The materials which are usually used for MN incorporated into OLED are low-reactive metals such as gold, silver, aluminum or copper. The organic materials surrounding the MN can be also slightly altered, for example, the MN could be placed in HBL, in ETL, or on the border of them. Figure 1.10a provides some additional understanding on the materials, which could be used. The comparison between gold, silver and copper is carried out [34]. The largest amplitude peak is present from MN made of silver. Gold and copper provide peaks at much lower energy (higher wavelength). The peak of Cu is almost not pronounced at 1.8 eV. Silver particles were chosen in this work due to the largest and the narrowest peak. Dependence on surrounding is studied in [35] and present in the figure 1.10b. The refractive index is changing from 1 (purple), to 2 (black) with a step of 0.25. The results are obtained by Mie calculations for the constant 20 nm golden MN. The surrounding media cannot be changed as easy as a shape of size of the nanoparticle, but it is still important to take this parameter in account.

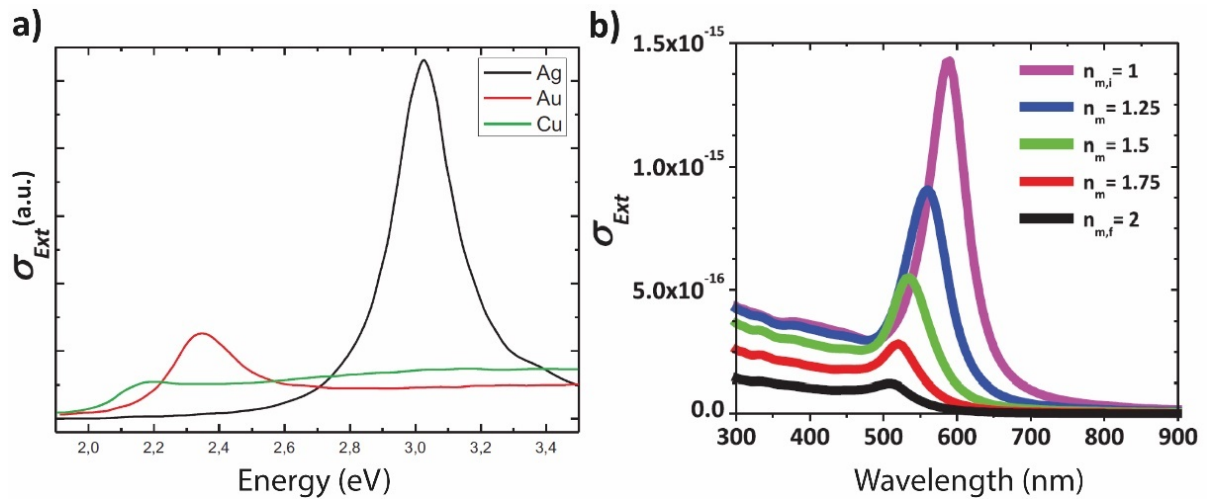


Fig. 1.10. Dependence of extinction spectra on a) the material of MN [34] and b) the surrounding media refractive index [35].

CHAPTER 2

SIMULATIONS OF THE LSPR

Many previous publications and studies about LSPR in the periodic metallic nanoparticles (PMN) have been provided in Chapter 1., but they do not perfectly match the conditions of the structures used in this work. Was decided to perform additional simulations for the structures that were planned to be exploited for the LSPR. There are various computational methods to solve Maxwell's equations, such as Mie model [32] and Yee's model called Finite difference time domain (FDTD) [36]. The latter was used in this work to simulate the behavior of the most interesting PMN structures.

2.1 Theory of FDTD

The FDTD method allows one to solve differential equations in different fields. In this work it is used to find electric \vec{E} and magnetic \vec{H} field by solving Maxwell's equations. The method is based on dividing or discretizing space and time and solving the equations in a unique way. A special volume area chosen of cubic shape where along edges the electric fields is solved and perpendicular to the sides the magnetic field is calculated (Fig. 2.1) [36]. The size of the cube is fixed and called a discretization step Δ delta.

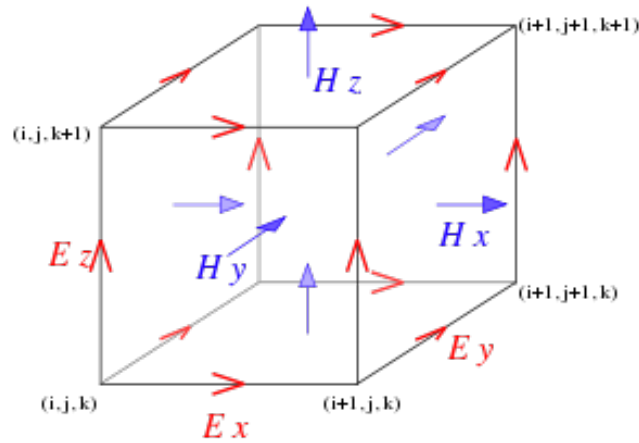


Fig. 2.1. Electric and magnetic fields in the elementary cell of Yee model [37].

The field elements U which are \vec{E} or \vec{H} in certain spatial x, y, z position can be solved by the following equations [1]. The time is also divided in time steps Δt .

$$U(x_i, y_j, z_k, t) = U_{i,j,k}^n \tag{2.1}$$

x_i, y_j, z_k are spatial positions where the field is calculated at the given moment t . Equation 2.2 provide partial time derivative and 2.3-2.5 are derivatives of the each dimension.

$$\left[\frac{\partial U}{\partial t}\right]_{i,j,k} = \frac{U_{i,j,k}^{n+\frac{1}{2}} - U_{i,j,k}^{n-\frac{1}{2}}}{\Delta t} \quad 2.2$$

$$\left[\frac{\partial U}{\partial x}\right]_{j,k,n} = \frac{U_{i+\frac{1}{2},j,k}^n - U_{i-\frac{1}{2},j,k}^n}{\Delta x} \quad 2.3$$

$$\left[\frac{\partial U}{\partial y}\right]_{i,k,n} = \frac{U_{i,j+\frac{1}{2},k}^n - U_{i,j-\frac{1}{2},k}^n}{\Delta y} \quad 2.4$$

$$\left[\frac{\partial U}{\partial z}\right]_{i,j,n} = \frac{U_{i,j,k+\frac{1}{2}}^n - U_{i,j,k-\frac{1}{2}}^n}{\Delta z} \quad 2.5$$

The main trick of the calculation model is not to solve both electric and magnetic fields at the same time, because they depend on each other. The leapfrog method is used in this case (Fig. 2.2). The electric field is calculated at the given moment t_0 , when the magnetic field is solved in the next moment $t_0+\Delta t$. The process is repeated the needed amount of times until all necessary conditions are met and the steady behavior of the electromagnetic field is reached [36].

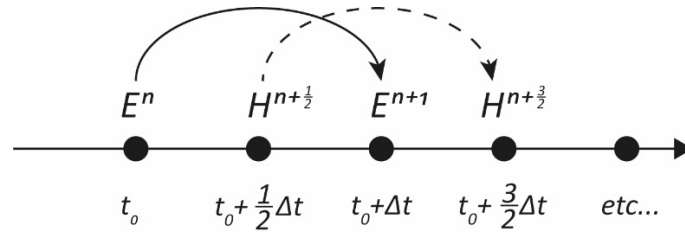


Fig. 2.2. The leapfrog method: time method of the Yee scheme. Reproduced from [1].

2.2 FDTD simulations

The FDTD method described above was used to simulate LSP resonance in the periodic structure of silver nanoparticles. The PMN was produced by e-beam lithography, so the closest approximation of the MN that were obtained after this procedure would be a cylindrical shape. The diameter and height of the cylinders is well controlled during the lithography. The nanoparticles are deposited on ITO as a first step before OLED production. Fig. 2.3 shows the schematic of the structure. The diameter and period of the structure are two main parameters that were simulated to see the effect on the LSPR. The period is the distance between 2 particles, when they are arranged in a square manner. As it was mentioned in Chapter 1, environment

characteristics affect the position of the absorption peak of the structure. In the simulations, the refractive index of the organic materials was set to 1.7. The simulations are kindly provided by Dr. Khadir.

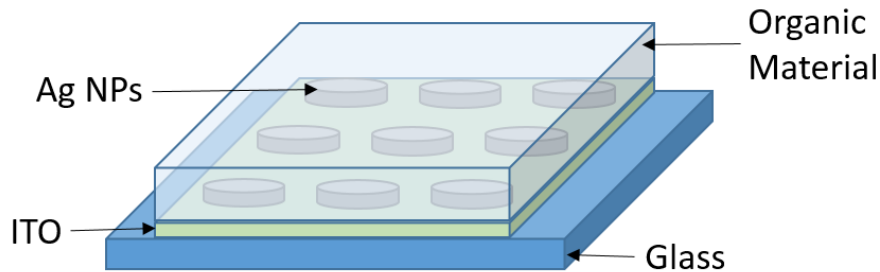


Fig. 2.3. Periodic metallic particles covered by organic material.

Simulation of particles with different diameter.

To decide what diameter of the particle is needed the FDTD simulations were applied to a single spherical silver nanoparticle. It is important to match the absorption peak of the LSP with the emission light of the device to achieve the resonance. Fig. 2.4. provides the results of simulation of single silver MN covered by media with $n=1.7$. The simulations for particles of size from 60 nm to 100 nm with a step of 10 nm were performed. The largest intensity peak corresponds to the largest particle and is centered at around 700 nm. With decreasing size, the peak is blue shifted down to 600 nm for the smallest 60 nm MN in diameter. These simulations do not fully represent the constructed MN from e-beam lithography, but help to realize how the size affects the LSPR.

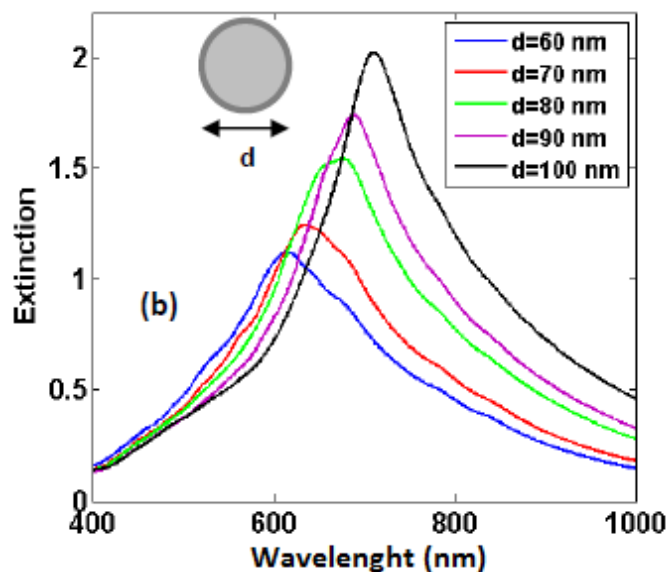


Fig. 2.4 Simulation of LSPR for different size of silver NP [1].

Simulation of structure with different period.

The period of the PMN is crucial in LSPR and also has been simulated. The simulations for 2 periods of 140 and 360 nm were performed. The results are presented in the Fig. 2.5. The main peak of the structure with period 360 is located at 850 nm and which is already in the infrared region. The main peak of PMN with a 140 nm period is centered at 700 nm but is much more broad. The experimental results (Fig. 3.6) showed slight disagreement with the simulated data, that is why the period of 360 was used in the experiment.

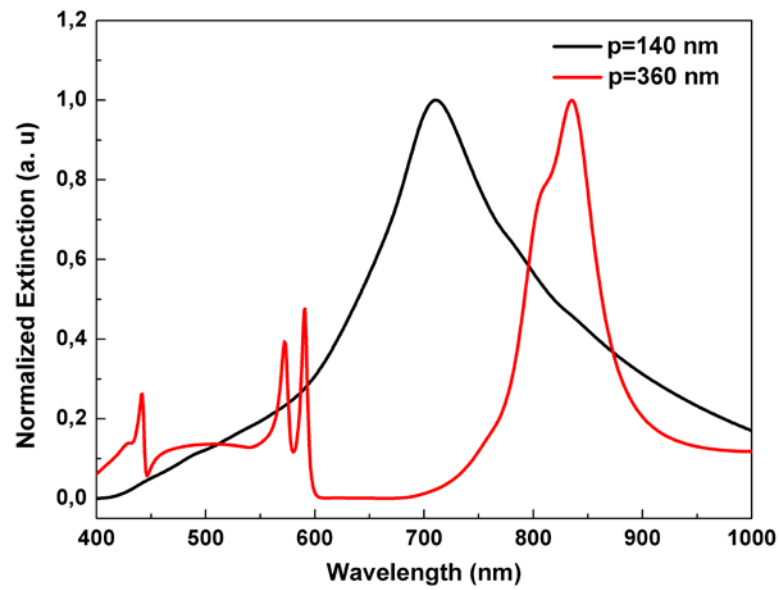


Fig. 2.5. Simulation of LSPR for different periods of silver NP structures.

CHAPTER 3

METHODOLOGY AND RESULTS

3.1 OLED production and measurement

There are many different methods that can be used to produce an OLED device. The 2 primary methods are spin coating and thermal evaporation. The spin coating is used for polymer organic semiconductors. The polymer OS is present in form of solution and can be spread on the surface of the device by the fast spinning. The time of spinning and speed will define what thickness of the solution left after. The advantages of this method is coverage of large areas, quick process and relatively easy procedure. The OS used in this work are composed of small molecules in comparison to polymers. Small molecule OS can be also deposited by spin coating as well as by the method of thermal evaporation. This method provides precise control over the thickness of deposited material. The deposition rate is also under control, which is needed in some situations. The technology of thermal evaporation was chosen in this work.

The OLED was deposited on commercially available glass substrate with Indium Tin Oxide (ITO) stripes. The substrates have dimensions of 25x17 mm, ITO is 150 nm thick with 15 Ω/cm^2 surface resistance. The substrates were purchased from LUMTEC. The connection between ITO and deposited layers of OS play a great role in the performance of the device. Special cleaning treatment was applied to the substrates to provide a perfectly clean interface between the first layer of organic (HIL) and ITO. Each samples followed the same steps of the cleaning procedure:

- Ultrasound bath: Acetone, 5 minutes;
- Ultrasound bath: Ethanol, 10 minutes;
- Ultrasound bath: Deionized water, 10 minutes;
- Rinse: Isopropanol, 5 minutes.

Cleaning of the substrates conducted in the clean room and clean samples were transferred to the evaporation chamber into high vacuum. The vacuum level in the chamber during deposition was around 10^{-7} mbar. The chamber had preloaded evaporation materials in powder form, such as organics and metals. The heating of crucibles was done by filament around them by applying direct current, the temperature was controlled by a specialized heating system. High temperature sublimates the material in the crucible and it condenses on the substrate.



Fig. 3.1. Evaporation chamber.

Evaporation chamber had installed a dedicated setup to control the deposition of the material. The control occurred *in situ* by means of a quartz detector. The working principle of the quartz detector is based on the measurements of frequency oscillations of the piezoelectric crystal. The detector was regularly cleaned to avoid wrong reading due to changes of oscillations of the crystal due to condensed on it materials.

The evaporation chamber included a setup that helped to produce OLEDs in an easy manner. There are 4 rotating plates with specific slits and openings that allowed to control the exposed area. Following rotating system was implemented:

- Substrate holder: a plate with two holders located on opposite sides (to avoid unwanted contaminations). Each holder allows to evaporate material on 8 samples;
- Mask plate: a mask holder with 8 sets of masks to deposit different materials on appropriate sample;
- Cover plate: a hiding plate allows to completely stop deposition;
- Crucible holder: A multi-crucible tray at the base of the chamber, which resides 8 crucibles, 6 of them OS and 2 for metals.

The evaporation chamber has two gates, one to operate it from outside and another to a glove box with inert gas. OS were introduced to the chamber from the glovebox to decrease contamination. The evaporation of organics is a very unstable process and needs to be carried out with extra care. The rise of temperature to evaporation point takes a relatively long time. The evaporation occurs at a rate of 0.2-0.3 nm/s. The sample was covered before stable deposition rate was achieved.

Each glass substrate has 4 ITO stripes with contact pads, which allows to create 4 OLEDs within one sample. The scheme of the substrate with devices is presented on figure 3.2. The organics are deposited on the desired areas, which are usually almost the entire substrate. The final step of deposition of Al cathode with 1 nm of LiF as an electron injection layer. The cathode utilizes a mask to form 4 OLEDs on the intersection between the ITO and Al. The AL-ITO intersection is $200 \times 100 \mu\text{m}^2$ developing micro or μ -OLED.

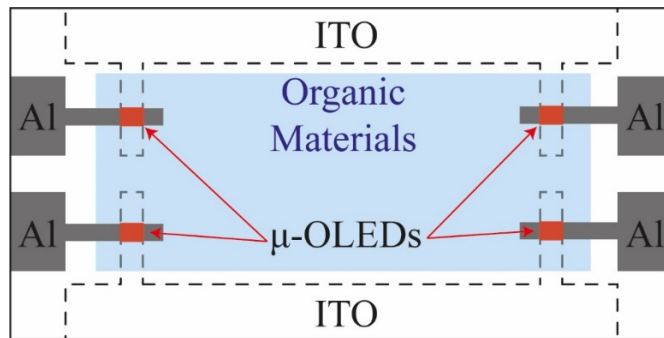


Fig. 3.2. Scheme of 4 OLED devices on a single glass substrate. Reproduced from [1].

The following organic materials were used in this experiment: ITO (Indium Tin oxide) as anode; m-MTDATA (4,4',4''-tris-(3-methylphenylphenylamino) triphenylamine) as hole injection layer (HIL) of 30 nm thickness; NPB (N, N'-Di(1-naphthyl)-N, N'-diphenyl-(1,1'-biphenyl)-4,4'-diamine) 15 nm as hole transport layer (HTL); Alq₃ doped with 1.5% 4-(dicyanomethylene)-2-methyl-6-(p-dimethylaminostyryl)-4H-pyran (DCM) as emitting layer (EM) for 30 nm; Holes blocking layer (HBL) is BCP (2,9-Dimethyl-4,7-diphenyl-1,10-phenanthroline) for 5 nm; Alq₃ (Tris-(8-hydroxyquinoline) aluminum) functions as electron transport layer (ETL) 30 nm; LiF (Lithium fluoride) for 1 nm and 100 nm Al (aluminum) cathode. The image of organic layers is presented on Figure 3.3.

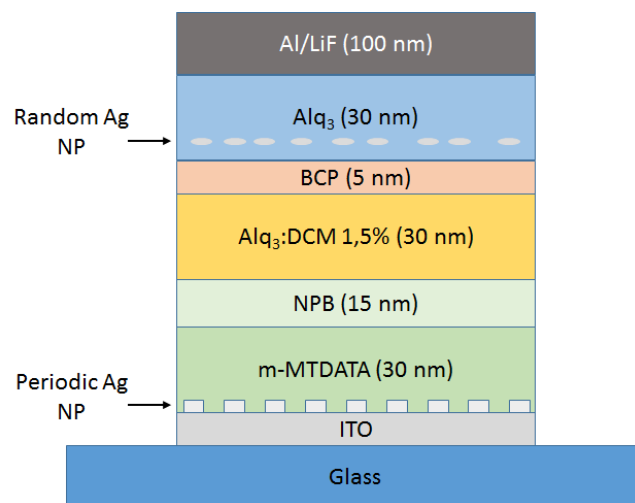


Fig. 3.3. Structure of organic layers of the OLED.

Prepared OLED devices were characterized with a confocal system within the laboratory. Due to the small size of μ -OLED the system resembles the microscopic setup. The design of the measuring setup is depicted on figure 3.4. The light from the OLED is accumulated by a 20x lens which through the system of lenses focuses it on the avalanche photodiode to measure the optic power or to the spectrometer. The spectrometer used in the measurements is Ocean Optics USB 2000 allows to determine the electroluminescence spectrum of the prepared device. The halogen lamp and a CCD camera is used to align the system before the measurements.

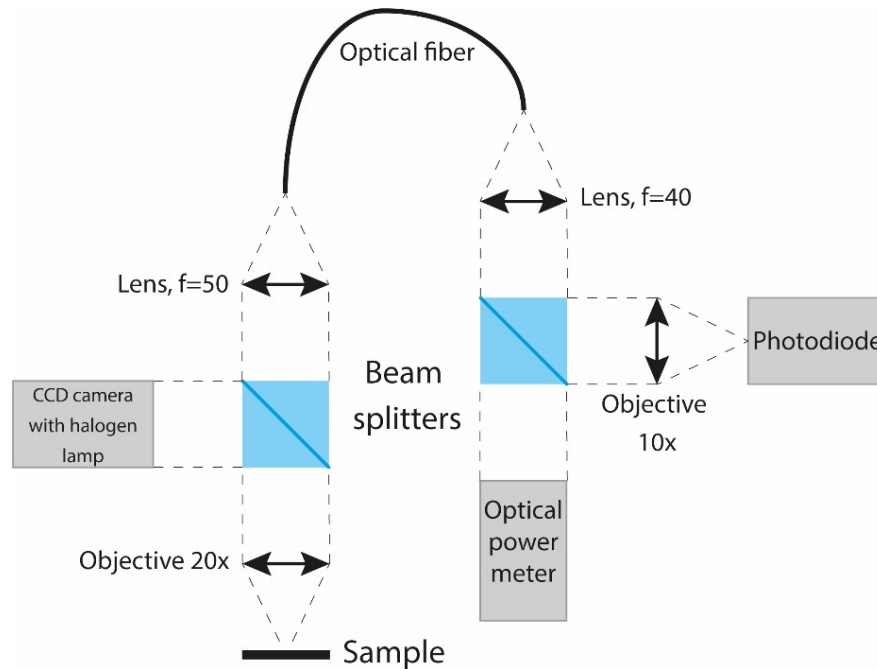


Fig. 3.4. Design of the characterization setup for μ -OLEDs. Reproduced from [1].

3.2 Fabrication of periodic nanostructures

To study the LSPR two different metallic nanostructures were encapsulated into the devices. Periodic metallic nanoparticles or PMN and random metallic nanoparticles – RMN. The latter were deposited by the process of thermal evaporation described above along with OLED production. To produce PMN electronic beam (e-beam) lithography was employed. The following section describes the principles of e-beam lithography.

The lithography process implies using a mask to obtain a certain pattern. In e-beam lithography the mask is produced with the help of an electronic beam. The beam is focused on the electron sensitive resist to crosslink (positive) or break the links (negative) in the special chemical film. The exposed area then can be removed (developed) to open up the surface for deposition of the desired material. The e-beam lithography has the main advantage over simpler optical lithography mostly in the resolution and precision. The resolution of optical lithography

is limited by the wavelength of used light [38]. The resolution of features down to 10 nm can be obtained by means of e-beam lithography. The process can be done on the electronic microscopes, in most of the cases on the scanning electron microscopes (SEM). The SEM has all utilities to focus the beam and navigate the sample for the purpose of lithography.

In this work the SEM Raith Pioneer was used along with available with it Pioneer software for mask design. PMMA (Poly (methyl methacrylate)) was used as a positive resist for the first step of lithography. The resin is coated on the sample by spin coating at 4500 rot/s and developed on the hot plate at 180°C for 5 minutes. The e-beam breaks down the bonds in PMMA, irradiated areas then can be dissolved in developing solutions. The sample is then immersed for 2 minutes into the developing solution: MIBK (methyl isobutyl ketone)/IPA (isopropyl alcohol) 1:3. To remove the residues of the developer the sample is ledt in isopropanol for 5 minutes and rinsed in the deionized water. Silver for MN of 35 nm is deposited in the same evaporation chamber where OLEDs are produced. The following step is lift-off – Acetone dissolves the resin PMMA (1 hour) under the deposited metal which removes the excess metal. This summarizes the e-beam process, which takes around the entire working day. The photo of the SEM used for the e-beam lithography and the step by step layout of the process is presented on figure 3.5.

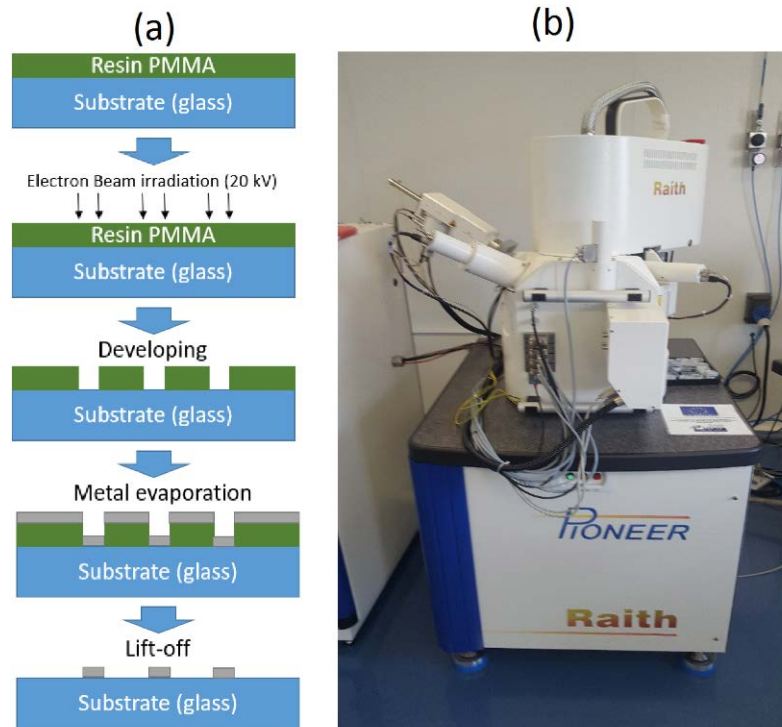


Fig. 3.5. (a) Summary diagram of e-beam lithography. (b) Scanning electron microscope Raith Pioneer at Paris 13.

3.3 Results and discussion

Nanostructure extinction results

Firstly, we had to confirm the simulation results and choose the appropriate period of the PMN structure. Samples with identical particles of 100 nm in diameter and 35 nm height, but with different periods of the pattern were produced with e-beam lithography. The periods varied from 250 nm to 400 nm with a step of 50 nm to find an appropriate period. The strong dependence of extinction peaks on period of nanostructure is observed. The extinction results are presented on figure 3.6 a and SEM overview image is on figure 3.6b. With the increasing of the period one can notice the red shift of the first mode peak. For production of red μ -OLED was chosen the PMN with a period of 360 nm where the biggest extinction peak is located at 620 nm. Unfortunately, the simulation was not in very good agreement with the experimental results, probably due to usage of spherical particles in the simulation, but other reasons could also have affected the results.

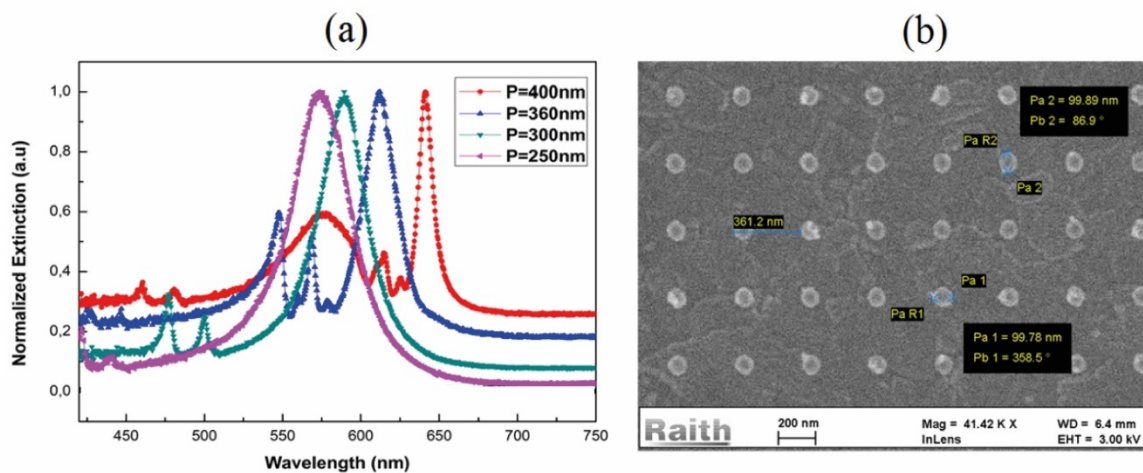


Fig. 3.6. (a) Extinction cross-section of silver nanoparticles with different periods. (b) SEM image of NS 100x100 nm with 360nm period.

OLED results

The final goal of the project was to produce OLED devices with periodic and random nanostructures to compare the effect of presence of LSPR on electric and light efficiency. Three final samples with NP and one reference OLED have the same organic structure as shown on figure 3.3. First sample contains only periodic structure, the second one has only random particles (RMN), the third sample has both types of nanoparticles. Silver RMN were deposited 15 nm away from the emitting layer into electron transport layer at the rate of 0.1 nm/s for 1 nm thickness. Silver 1 nm film does not create a continuous surface but agglomerates to nanoparticles with an approximate size of 1-10 nm, which was confirmed previously in the lab.

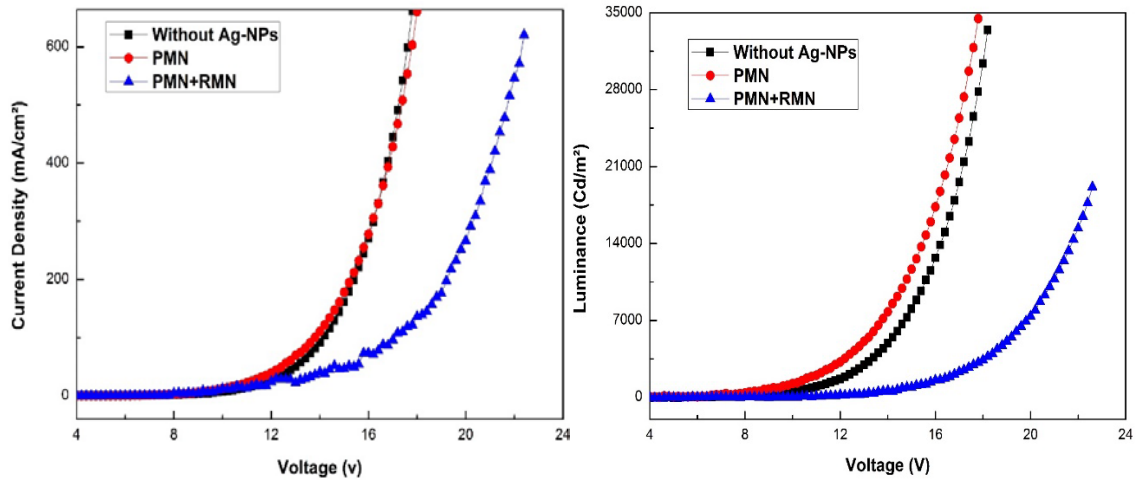


Fig. 3.7 (a) Current density and (b) luminance as a function of the voltage for the μ -OLEDs with and without Ag NPs.

The current density and luminance characteristics as a function of the voltage of the μ -OLEDs with and without the NPs are shown in Figure 3.7. Was found that the current density of the μ -OLED incorporating the silver PMN and RMN is much lower than that of the reference device. Luminescence of the OLED with PMN is greater than a reference device in contrast to the OLED with PMN and PMN. The results of the device with only RMN are not presented due to unexpected data. The devices with RMN have been corrupted during the production.

Efficiency of these OLEDs is plotted on Figure 3.8. The efficiency of OLED with PMN is up to 20% higher in comparison to the reference device at the same current density. At the same time, the OLED with both types of nanostructures claims slightly worse results.

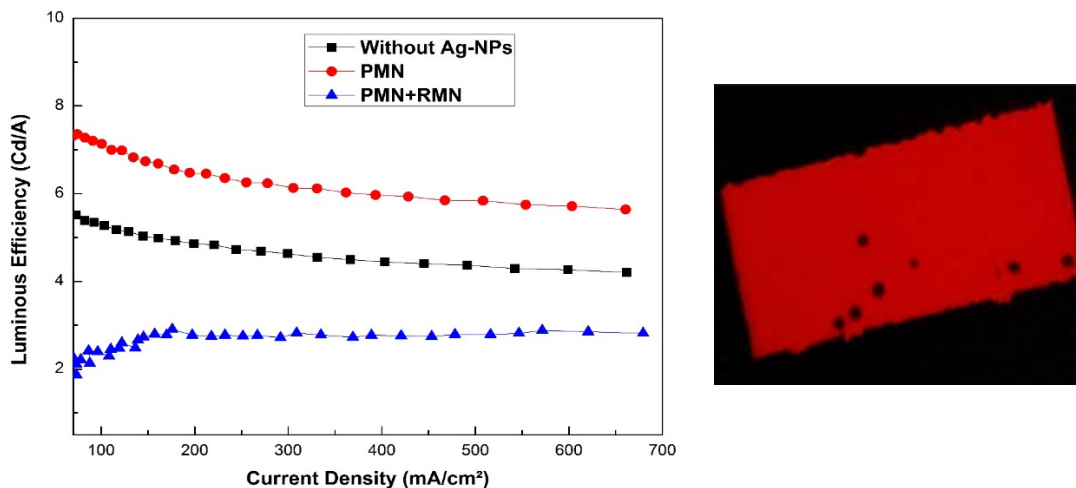


Fig. 3.8. Luminous efficiency as a function of current density (left), image of the reference red OLED (right).

CONCLUSION

The work aimed to answer the question how the periodic and random structures of nanoparticles affect the performance of OLED devices and to what extent the LSPR will increase the efficiency. The simulations using FDTD calculational method were used to predict the LSPR behavior on the desired structures. Even though the predicted results resemble the same shape of the LSPR, but peak positions were shifted. It could have happened due to a slightly different simulated system and prepared PMN structure. To study the problem red OLEDs were chosen for production as one of the most reliable devices. Silver NP for both PMN and RMN were appointed for the task of LSPR. The devices with defined organic content and different addition of metallic nanoparticles were produced with high effort. Obtained OLEDs were of high quality and were measured without additional complications. 3 final devices of each type were characterized, including the reference device without MN, the device with only PMN structure and the last device with PMN and RMN structures on the both sides of the emitting layer. The finding claims that the device with only PMN demonstrated a 20% increase in efficiency compared to the reference OLED. Such behavior was expected because similar devices were previously produced in the lab with similar results. The positive result is fully attributed to the LSPR. The device with both PMN and RMN structures did not exhibit any improvement, the efficiency has reduced by almost 50%. Encapsulated random particles, which are 1 nm of silver in the electron transport layer, could have affected the transport properties of Alq₃ and decrease the overall quality of the OLED. Another reason for the decreased efficiency of the OLED with both structures could be the presence of silver particles on both sides of the emitting layer, having RMN on the same side as PMN could have changed the outcome of the experiment.

Unfortunately, we could not continue this study due to lack of time. Further research is needed not only to experiment with the position and distance between RMN and EL, but also better understanding of PMN structures, reasons for different modes in the extinction graphs. Such understanding will help future scientists to produce OLEDs with better quality.

REFERENCE LIST

- [1] S. Khadir, “Effets des résonances plasmon de surface localisé sur les performances optiques et électriques des diodes électroluminescentes organiques,” Université Mouloud Mammeri de Tizi-Ouzou, 2016.
- [2] W. L. Barnes, A. Dereux, and T. W. Ebbesen, “Surface plasmon subwavelength optics,” *Nature*, vol. 424, no. 6950, pp. 824–830, 2003.
- [3] C. W. Tang and S. A. Vanslyke, “Organic electroluminescent diodes,” *Appl. Phys. Lett.*, vol. 51, no. 12, pp. 913–915, 1987.
- [4] M. C. Gather, A. Köhnen, and K. Meerholz, “White organic light-emitting diodes,” *Adv. Mater.*, vol. 23, no. 2, pp. 233–248, Jan. 2011.
- [5] N. B. Hannay and B. R. Sundheim, “Semiconductors,” *J. Electrochem. Soc.*, vol. 106, no. 8, p. 226Cb, Aug. 1959.
- [6] M. Pope, H. P. Kallmann, and P. Magnante, “Electroluminescence in organic crystals,” *J. Chem. Phys.*, vol. 38, no. 8, pp. 2042–2043, 1963.
- [7] F. C. Chen, *Organic semiconductors*, vol. 1–5. Malabar, Florida: R. E. Krieger, 2018.
- [8] M. Pope and C. E. Swenberg, “Electronic processes in organic crystals and polymers / Martin Pope, Charles E. Swenberg,” *Oxford Univ. Press USA 2nd Ed.*, 1999.
- [9] S. Hameed, P. Predeep, and M. R. Baiju, “Polymer light emitting diodes - A review on materials and techniques,” *Rev. Adv. Mater. Sci.*, vol. 26, no. 1–2, pp. 30–42, 2010.
- [10] J. Li and D. Liu, “Dendrimers for organic light-emitting diodes,” *J. Mater. Chem.*, vol. 19, no. 41, pp. 7584–7591, 2009.
- [11] E. B. Namdas, T. D. Anthopoulos, I. D. W. Samuel, M. J. Frampton, S. C. Lo, and P. L. Burn, “Simple color tuning of phosphorescent dendrimer light emitting diodes,” *Appl. Phys. Lett.*, vol. 86, no. 16, pp. 1–3, Apr. 2005.
- [12] B. Geffroy, P. le Roy, and C. Prat, “Organic light-emitting diode (OLED) technology: Materials, devices and display technologies,” *Polym. Int.*, vol. 55, no. 6, pp. 572–582, Jun. 2006.
- [13] J. Shinar, *Organic Light-Emitting Devices*. AIP press, 2004.

- [14] Y. Zhou *et al.*, “Direct correlation between work function of indium-tin-oxide electrodes and solar cell performance influenced by ultraviolet irradiation and air exposure,” *Phys. Chem. Chem. Phys.*, vol. 14, no. 34, pp. 12014–12021, Aug. 2012.
- [15] V. M. Manninen, W. A. E. Omar, J. P. Heiskanen, H. J. Lemmetyinen, and O. E. O. Hormi, “Synthesis and characterization of tris-(5-amino-8-hydroxyquinoline)aluminum complexes and their use as anode buffer layers in inverted organic solar cells,” *J. Mater. Chem.*, vol. 22, no. 43, pp. 22971–22982, 2012.
- [16] F. Li, Y. Zhang, C. Wu, Z. Lin, B. Zhang, and T. Guo, “Improving efficiency of organic light-emitting diodes fabricated utilizing AZO/Ag/AZO multilayer electrode,” *Vacuum*, vol. 86, no. 12, pp. 1895–1897, Jul. 2012.
- [17] S. Negi, P. Mittal, and B. Kumar, “Impact of different layers on performance of OLED,” *Microsyst. Technol.*, vol. 24, no. 12, pp. 4981–4989, 2018.
- [18] P. K. Bhatnagar, “Organic Light-Emitting Diodes—A Review,” pp. 261–287, 2018.
- [19] T. F. Guo, F. S. Yang, Z. J. Tsai, T. C. Wen, S. N. Hsieh, and Y. S. Fu, “High-performance polymer light-emitting diodes utilizing modified Al cathode,” *Appl. Phys. Lett.*, vol. 87, no. 1, 2005.
- [20] H. Y. Cho, E. J. Park, J. H. Kim, and L. S. Park, “Effect of hole injection layer/hole transport layer polymer and device structure on the properties of white OLED,” *J. Nanosci. Nanotechnol.*, vol. 8, no. 10, pp. 4916–4922, 2008.
- [21] E. Bellmann *et al.*, “New Triarylamine-Containing Polymers as Hole Transport Materials in Organic Light-Emitting Diodes: Effect of Polymer Structure and Cross-Linking on Device Characteristics,” *Chem. Mater.*, vol. 10, no. 6, pp. 1668–1676, 1998.
- [22] Y. Sato, S. Ichinosawa, and H. Kanai, “Operation characteristics and degradation of organic electroluminescent devices,” *IEEE J. Sel. Top. Quantum Electron.*, vol. 4, no. 1, pp. 40–48, Jan. 1998.
- [23] F. B. Dias *et al.*, “Triplet harvesting with 100% efficiency by way of thermally activated delayed fluorescence in charge transfer OLED emitters,” *Adv. Mater.*, vol. 25, no. 27, pp. 3707–3714, Jul. 2013.

- [24] R. M. Clegg, "Fluorescence resonance energy transfer," *Chemical Analysis*, 1996. [Online]. Available: <https://chem.libretexts.org/@go/page/2012>.
- [25] U. of California, "Dexter Energy Transfer - Chemwiki," 2011. [Online]. Available: http://chemwiki.ucdavis.edu/Theoretical_Chemistry/Fundamentals/Dexter_Energy_Transfer.
- [26] P. E. Burrows, V. Bulovic, S. R. Forrest, L. S. Sapochak, D. M. McCarty, and M. E. Thompson, "Reliability and degradation of organic light emitting devices," *Appl. Phys. Lett.*, vol. 65, no. 23, pp. 2922–2924, Jun. 1994.
- [27] M. Schaer, F. Nüesch, D. Berner, W. Leo, and L. Zuppiroli, "Water vapor and oxygen degradation mechanisms in organic light emitting diodes," *Adv. Funtional Mater.*, vol. 11, no. 2, pp. 116–121, 2001.
- [28] S. Scholz, D. Kondakov, B. Lüssem, and K. Leo, "Degradation mechanisms and reactions in organic light-emitting devices," *Chem. Rev.*, vol. 115, no. 16, pp. 8449–8503, 2015.
- [29] F. So and D. Kondakov, "Degradation mechanisms in small-molecule and polymer organic light-emitting diodes," *Adv. Mater.*, vol. 22, no. 34, pp. 3762–3777, Sep. 2010.
- [30] K. A. Willets and R. P. Van Duyne, "Localized surface plasmon resonance spectroscopy and sensing," *Annu. Rev. Phys. Chem.*, vol. 58, pp. 267–297, 2007.
- [31] V. Amendola, O. M. Bakr, and F. Stellacci, "A study of the surface plasmon resonance of silver nanoparticles by the discrete dipole approximation method: Effect of shape, size, structure, and assembly," *Plasmonics*, vol. 5, no. 1, pp. 85–97, Jan. 2010.
- [32] C. Noguez, "Surface plasmons on metal nanoparticles: The influence of shape and physical environment," *J. Phys. Chem. C*, vol. 111, no. 10, pp. 3606–3619, Mar. 2007.
- [33] J. J. Mock, M. Barbic, D. R. Smith, D. A. Schultz, and S. Schultz, "Shape effects in plasmon resonance of individual colloidal silver nanoparticles," *J. Chem. Phys.*, vol. 116, no. 15, pp. 6755–6759, 2002.
- [34] M. Hamidi, "Modélisation par la méthode FDTD des plasmons de surface localisés," Université Mouloud Mammeri de Tizi-Ouzou, 2012.

- [35] V. Amendola, R. Pilot, M. Frasconi, O. M. Maragò, and M. A. Iatì, “Surface plasmon resonance in gold nanoparticles: A review,” *J. Phys. Condens. Matter*, vol. 29, no. 20, 2017.
- [36] K. Yee, “Numerical Solution of Initial Boundary Value Problems Involving Maxwell’s Equations in Isotropic Media,” 1966.
- [37] Wikipedia, “Метод конечных разностей во временной области,” 2021. [Online]. Available:
https://ru.wikipedia.org/wiki/Метод_конечных_разностей_во_временной_области.
- [38] F. L. Somer, “Nanophysics and Nanotechnology: An Introduction to Modern Concepts in Nanoscience (Wolf, Edward L.),” *J. Chem. Educ.*, vol. 82, no. 11, p. 1625, Nov. 2005.